

High-spin states and band terminations in ^{49}V

D. Rodrigues,^{1,2,3,*} D. Hojman,^{1,2} S. M. Lenzi,⁴ M. A. Cardona,^{1,2,5} E. Farnea,⁴ M. Axiotis,⁶ C. Beck,⁷ P. Bednarczyk,⁸ P. G. Bizzetti,⁹ A. M. Bizzetti-Sona,⁹ F. Della Vedova,⁴ J. Grębosz,⁸ F. Haas,⁷ M. Kmiecik,⁸ A. Maj,⁸ W. Męczyński,⁸ D. R. Napoli,⁶ M. Nespolo,⁴ P. Papka,⁷ A. Sánchez i Zafra,⁷ J. Styczen,⁸ S. Thummerer,¹⁰ and M. Ziębliński⁸

¹*Departamento de Física, Comisión Nacional de Energía Atómica, BKNA1650 San Martín, Argentina*

²*CONICET, C1033AAJ Buenos Aires, Argentina*

³*Departamento de Física, FCEyN, Universidad de Buenos Aires, 1428 Buenos Aires, Argentina*

⁴*Dipartimento di Fisica e Astronomia dell'Università and INFN, Sezione di Padova, I-35131 Padova, Italy*

⁵*Escuela de Ciencia y Tecnología, Universidad de San Martín, BKNA1650 San Martín, Argentina*

⁶*INFN, Laboratori Nazionali di Legnaro, I-35020 Legnaro, Italy*

⁷*IPHC, CNRS, IN2P3 and Université de Strasbourg, F-67037 Strasbourg Cedex 2, France*

⁸*The Henryk Niewodniczański Institute of Nuclear Physics, Polish Academy of Sciences, 31-342 Kraków, Poland*

⁹*Dipartimento di Fisica dell'Università and INFN, Sezione di Firenze, I 50019 Firenze, Italy*

¹⁰*Helmholtz-Zentrum Berlin, 14109 Berlin, Germany*

(Received 15 June 2015; published 27 August 2015)

High-spin states in ^{49}V have been studied through the $^{28}\text{Si}(^{28}\text{Si}, \alpha 3p)$ reaction using the EUROBALL γ -ray detector array. The ^{49}V level scheme has been extended up to 13.1 MeV including 21 new states. Both negative and positive parity states have been interpreted in the framework of the shell model. The $27/2^-$ and the $31/2^+$ band-termination states have been observed in agreement with theoretical predictions.

DOI: [10.1103/PhysRevC.92.024323](https://doi.org/10.1103/PhysRevC.92.024323)

PACS number(s): 21.10.Hw, 21.60.Cs, 23.20.Lv, 27.40.+z

I. INTRODUCTION

Nuclei in the middle of the $1f_{7/2}$ shell have been widely studied both theoretically and experimentally. These nuclei present sizable deformation near the ground state [1–6]. In particular, ^{48}Cr is considered to be the best rotor in this shell with a deformation parameter $\beta \approx 0.28$ [1,3,4,6,7]. Shell model calculations in the full fp shell [8,9] reproduce with good agreement the new experimental data. In addition, high-efficiency detector arrays have allowed the study of relatively light nuclei at high spins.

Furthermore, investigations on several nuclei in the middle of the $1f_{7/2}$ shell were focused on the yrast sequence of levels up to the smooth band termination for natural and unnatural parity. The interplay between single particle and collective degrees of freedom is clearly exhibited and manifested in backbending and band-termination phenomena. The occurrence of high-energy transitions connecting the band-termination state with states of higher angular momentum could be considered as an indicator of the band-termination process in this mass region [10]. The arguments usually applied to explain phenomena such as backbending and changes of shape in heavier nuclei cannot be directly extrapolated to the $A \sim 50$ mass region. These properties, however, can be understood in terms of the dynamical evolution of the structure with increasing excitation energy and angular momentum. Neutron-proton correlations have a crucial role because valence nucleons are filling the same shell [2]. Band-terminating states are developed when all the valence particles are aligned with the rotational axis. It happens by breaking pairs of valence nucleon forced by the

high excitation energy and spin as a mechanism to generate angular momentum [11,12].

High-spin spectroscopy in this mass region is a nontrivial task for many reasons. In a fusion-evaporation reaction, the light masses of the reaction partners restrict the angular momentum of the compound nucleus. Furthermore, high spin states decay via relatively high energy γ -rays which are usually detected with low efficiency. Symmetrical reactions are needed to populate high spin states. This implies large recoil velocities. In addition, the evaporation of light particles induce large deviations of the velocity vectors of the residual nuclei. Consequently, Doppler corrections are affected by large uncertainties in the emission angle of the γ -ray transitions relative to the direction of the emitter resulting in substantial broadening. Furthermore, light nuclei present a low Coulomb barrier to light charged particles resulting in a large number of open channels from the deexcitation of highly excited compound nuclei.

Therefore, the simultaneous detection of recoiling nuclei or evaporated particles and γ -rays with high efficiency provides a powerful technique for selecting the individual channels and for reconstructing event by event the kinematics, resulting in an improvement in γ -energy resolution.

In this context, we have studied the high spin states in ^{49}V with a selective detector setup characterized by high efficiency and high resolution. As a result we have extended the level scheme up to $E_x = 13.1$ MeV, reporting 21 states and 51 transitions for the first time. Previous studies at high spin have been performed by Cameron *et al.* [13] through the $^{12}\text{C} + ^{40}\text{Ca}$ reaction.

In Sec. II we describe the experimental and data analysis details, together with the adopted level scheme. The discussion

*darodrig@tandar.cnea.gov.ar

of the results and its comparison with theoretical calculations is presented in Sec. III. Finally, conclusions are given in Sec. IV.

II. MEASUREMENTS AND RESULTS

A. Experimental details

High-spin states in ^{49}V have been populated through the $^{28}\text{Si}(^{28}\text{Si},\alpha 3p)$ fusion-evaporation reaction at a bombarding energy $E_{\text{lab}}(^{28}\text{Si}) = 117$ MeV. The beam was provided by the Vivitron accelerator installed at IReS, Strasbourg, France. The target consisted of two $200 \mu\text{g}/\text{cm}^2$ ^{28}Si stacked foils enriched to 99.9%.

The γ -rays were detected with the EUROBALL IV [14] multidetector array, composed of 15 cluster detectors and 26 clover detectors. In addition, the Recoil Filter Detector (RFD) [15] was used to measure the velocity vector of the recoiling nuclei and to perform an event-by-event Doppler correction of the energies of the detected γ -rays.

The RFD system is a set of 18 fast heavy ion detectors placed at a distance of 1.34 m from the target and arranged in three concentric rings around the beam axis. They cover an azimuth angular range of 2–7 degrees with respect to the beam axis. Such a geometry is optimum for catching recoiling evaporation residua, that are typically detected with 40% efficiency, whereas 99.9% of projectiles pass through the central hole and are stopped in a distant beam dump. Each RFD element consists of a thin aluminized mylar foil which emits secondary electrons whenever a recoiling nucleus impales on its surface. Those electrons are accelerated and focused by an electrostatic field generated by a series of annular electrodes on a thin plastic scintillator connected to a photomultiplier and a fast preamplifier. The output signal is proportional to the number of secondary electrons, thus to the energy loss of the detected heavy ion. The time of flight, defined with respect to the radio frequency of the pulsed beam, and the detector position allow to reconstruct the velocity vector of each recoil nucleus, that can be used for event-by-event Doppler correction of the coincident γ -rays. In this experiment the mean recoil velocity of the ^{49}V evaporation residua was $v/c = 0.04$; when applying this value for a Doppler correction, from a summed γ spectrum of all the EUROBALL Ge detectors, an average FWHM of 12 keV for a 1.3 MeV transition was obtained. In contrast, event-by-event Doppler correction using the RFD information resulted in significant improvement of the energy resolution, that was FWHM = 6 keV at 1.3 MeV.

Events were collected with a trigger condition of at least two Ge detector elements and the RFD in coincidence. Add-back mode was used in sorting all of the cluster and clover event data. After the unfolding, the number of double and triple γ -coincidence events was 6.3×10^8 and 1.6×10^8 , respectively. We constructed two symmetrized matrices: E_γ - E_γ and E_γ - E_γ - E_γ , and an asymmetric matrix for angular distributions to obtain the DCO ratios (R_{DCO}) [16]. The DCO ratios of a selected transition were determined from its γ -ray intensities measured in coincidence spectra, according to the relation

$$R_{\text{DCO}} = \frac{I_{\gamma_{\text{gate}=\theta_2}}(\theta_1)}{I_{\gamma_{\text{gate}=\theta_1}}(\theta_2)},$$

where $\langle\theta_1\rangle = 156^\circ$ and $\langle\theta_2\rangle = 90^\circ$. In the EUROBALL geometry, setting gates on stretched quadrupole transitions leads to theoretical $R_{\text{DCO}} \approx 0.6$ for $\Delta I = 1$ pure dipole transitions and $R_{\text{DCO}} \approx 1$ for stretched quadrupole or $\Delta I = 0$ pure dipole transitions. A dealignment parameter $\sigma/I = 0.3$ is used for the prompt transitions.

B. Level scheme

The level scheme proposed for ^{49}V is shown in Fig. 1. It has been extended up to 13.1 MeV and consists of 39 excited states and 87 transitions, from which 21 states and 51 transitions have been observed for the first time. The assignment of transitions to ^{49}V was based on triple γ -coincidences setting gates on clean transitions previously assigned to ^{49}V [17]. Despite the large number of open channels in the $^{28}\text{Si} + ^{28}\text{Si}$ reaction (see Fig. 2), the statistics obtained for ^{49}V was good enough to select clean triple γ -coincidence events. The level scheme reported by Cameron *et al.* [13] is confirmed in the present work with the exception of the states located at 2672 keV and 8414 keV. Several transitions have not been observed and others are placed otherwise in the level scheme.

Transition energies, initial-level energies, γ -ray intensities, spin and parity assignments, and DCO ratios are listed in Table I. Spin and parity assignments have been based on previous investigations [17], coincidence relationships, and DCO ratios. Spins and parities reported in the level scheme and Table I between parentheses are tentatively assigned based on the comparison with theoretical calculations and on the systematics. Figure 3 displays the experimental DCO ratios obtained in this work.

The proposed level scheme is basically composed of three parts. The main structure is the negative-parity yrast band which extends up to the maximum spin that can be built with three protons and six neutrons in the $f_{7/2}$ shell, i.e., the band-terminating $27/2^-$ state at 7.8 MeV. Another structure consists of positive parity states starting on the $3/2^+$ state at 748 keV. A third structure can be seen in the right upper part of the level scheme, where spins and parities could not be unambiguously determined.

Figure 4 shows coincidence spectra doubly gated on selected transitions belonging to ^{49}V . Panel (a) shows the spectrum gated on the two strongest transitions of the level scheme (1021.6 and 1241.2 keV γ -rays). Apart from the transitions belonging to the ground state band, the strongest transitions in the high spin structure on the upper right part of the level scheme (marked with *) are observed. Most of the high energy transitions feeding the ground-state structure are observed as well, and are absent in panel (b) where the gates are set on the lower and higher transitions of the ground-state band (955.5 and 1021.6 keV γ -rays). Panel (c) shows evidence of positive parity structure; this spectrum is obtained setting gates on the 1138.5 and 1340.8 keV transitions. Panel (d) displays the spectrum gated on the 634.3 and 701.8 keV γ -rays belonging to the third structure in the right upper part of the level scheme. In addition to the in-band lines, this spectrum shows the transitions linking this structure with the yrast states.

For the latter mentioned structure, the adopted spins correspond to the highest values compatible with the

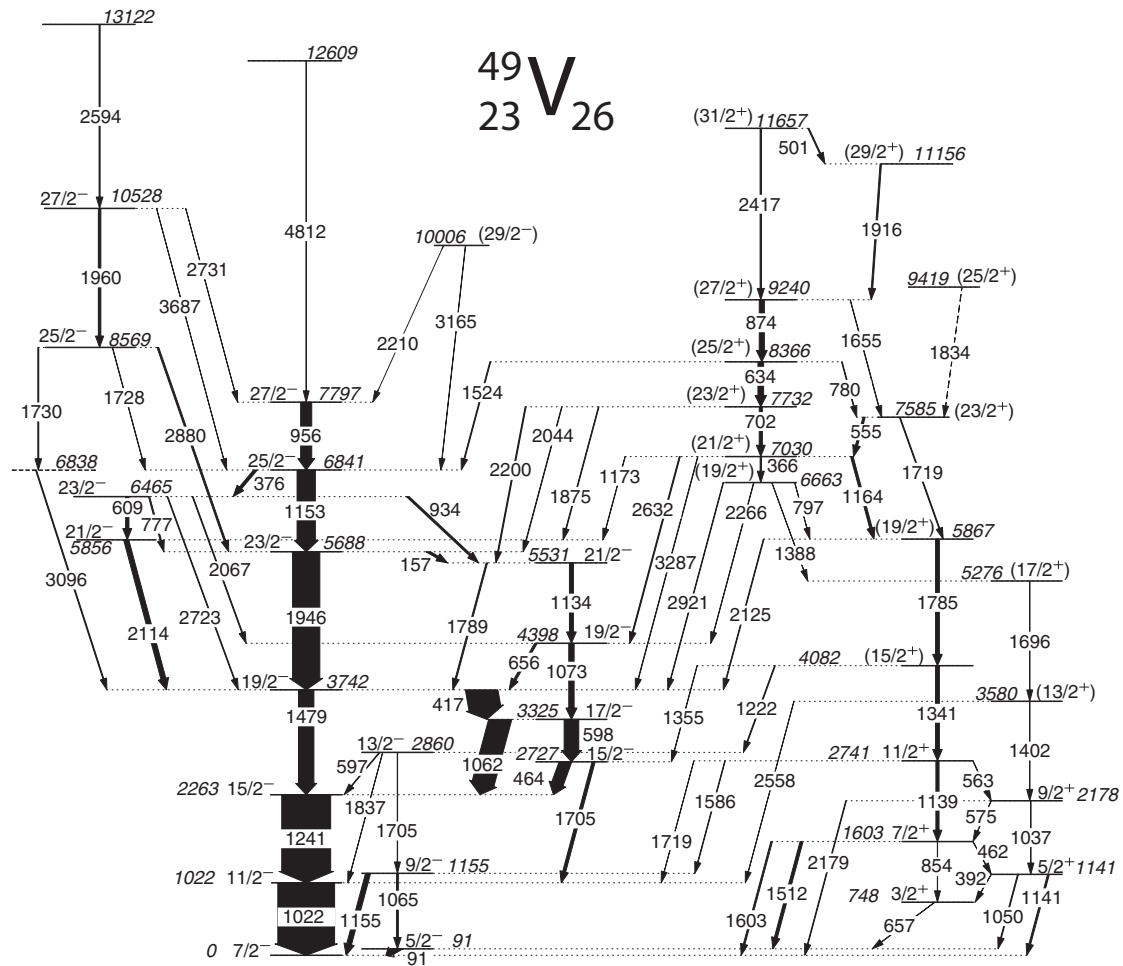


FIG. 1. Level scheme proposed for ^{49}V .

DCO analysis and decay pattern. Regarding the parity, since the 634.3 and 874.2 keV transitions are the most intense lines above the band termination of the negative parity yrast band, the positive parity sequence is adopted.

The order of the 1730 and 3096 keV transitions, linking the 8568.5 and 3742.0 keV states, could not be determined due to the similar intensities of the transitions and because no transitions from the intermediate state were observed. We adopted the order shown in the level scheme since a 3102 keV transition

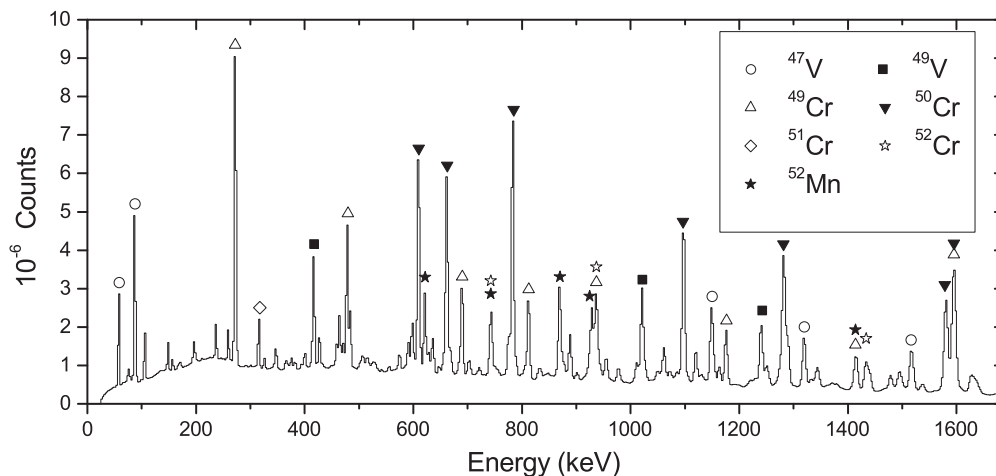


FIG. 2. Projection of the E_γ - E_γ - E_γ matrix obtained with EUROBALL in conjunction with the RFD for the $^{28}\text{Si} + ^{28}\text{Si}$ reaction. The assignment of the strongest lines is indicated.

TABLE I. γ -ray energy, initial-level energy, γ -ray intensity, spin and parity assignment, and DCO ratio of transitions of ^{49}V .

E_γ (keV)	E_i (keV)	I_γ^a	$I_i^\pi \rightarrow I_f^\pi$	R_{DCO}^b
90.6(2)	90.7	102(15)	$5/2^- \rightarrow 7/2^-$	0.37(18)
156.6(3)	5688.1	51(3)	$23/2^- \rightarrow 21/2^-$	0.38(5)
366.2(4)	7029.8	23(2)	$(21/2^+) \rightarrow (19/2^+)$	0.33(15)
375.7(2)	6841.0	50(3)	$25/2^- \rightarrow 23/2^-$	0.52(8)
392.3(6)	1140.6	3(1)	$5/2^+ \rightarrow 3/2^+$	
416.8(2)	3742.0	565(15)	$19/2^- \rightarrow 17/2^-$	0.45(2)
462.1(5)	1602.7	6(2)	$7/2^+ \rightarrow 5/2^+$	
464.1(2)	2726.9	210(8)	$15/2^- \rightarrow 15/2^-$	1.08(5)
501.3(4)	11656.8	19(3)	$(31/2^+) \rightarrow (29/2^+)$	
555.4(4)	7585.1	37(4)	$(23/2^+) \rightarrow (21/2^+)$	0.41(10)
563.2(5)	2741.2	6(3)	$11/2^+ \rightarrow 9/2^+$	
574.9(6)	2178.0	5(2)	$9/2^+ \rightarrow 7/2^+$	
597.0(5)	2859.9	11(3)	$13/2^- \rightarrow 15/2^-$	
598.1(2)	3325.2	258(9)	$17/2^- \rightarrow 15/2^-$	0.51(3)
609.2(3)	6465.4	58(4)	$23/2^- \rightarrow 21/2^-$	0.58(5)
634.3(3)	8365.7	100(6)	$(25/2^+) \rightarrow (23/2^+)$	0.48(3)
655.7(3)	4397.9	39(4)	$19/2^- \rightarrow 19/2^-$	1.47(13)
657.0(7)	748.1	5(2)	$3/2^+ \rightarrow 5/2^-$	
701.8(3)	7731.5	55(5)	$(23/2^+) \rightarrow (21/2^+)$	0.67(17)
777.4(4)	6465.4	21(4)	$23/2^- \rightarrow 23/2^-$	1.04(7)
780.3(6)	8365.7	12(5)	$(25/2^+) \rightarrow (23/2^+)$	
796.9(6)	6663.4	4(2)	$(19/2^+) \rightarrow (19/2^+)$	
854.3(7)	1602.7	4(2)	$7/2^+ \rightarrow 3/2^+$	
874.2(3)	9240.0	90(6)	$(27/2^+) \rightarrow (25/2^+)$	0.72(10)
934.4(4)	6465.4	35(2)	$23/2^- \rightarrow 21/2^-$	0.76(15)
955.5(3)	7796.5	195(6)	$27/2^- \rightarrow 25/2^-$	0.49(3)
1021.6(2)	1021.6	1000(83)	$11/2^- \rightarrow 7/2^-$	0.90(4)
1037.3(8)	2178.0	10(4)	$9/2^+ \rightarrow 5/2^+$	
1050.0(6)	1140.6	15(4)	$5/2^+ \rightarrow 5/2^-$	
1062.4(2)	3325.2	395(8)	$17/2^- \rightarrow 15/2^-$	0.48(2)
1064.6(6)	1155.1	31(8)	$9/2^- \rightarrow 5/2^-$	
1072.9(3)	4397.9	94(4)	$19/2^- \rightarrow 17/2^-$	0.39(7)
1133.6(4)	5531.3	70(4)	$21/2^- \rightarrow 19/2^-$	0.52(6)
1138.5(4)	2741.2	55(13)	$11/2^+ \rightarrow 7/2^+$	
1140.6(9)	1140.6	30(9)	$5/2^+ \rightarrow 7/2^-$	
1152.9(3)	6841.0	322(10)	$25/2^- \rightarrow 23/2^-$	0.46(2)
1155.2(5)	1155.1	86(10)	$9/2^- \rightarrow 7/2^-$	
1163.6(7)	7029.8	43(10)	$(21/2^+) \rightarrow (19/2^+)$	
1173(1)	7029.8	6(3)	$(21/2^+) \rightarrow 21/2^-$	
1222.2(6)	4082.0	14(5)	$(15/2^+) \rightarrow 13/2^-$	
1241.2(2)	2262.8	862(33)	$15/2^- \rightarrow 11/2^-$	1.01(4)
1340.8(4)	4082.0	68(14)	$(15/2^+) \rightarrow 11/2^+$	
1355.0(6)	4082.0	6(2)	$(15/2^+) \rightarrow 15/2^-$	
1387.7(7)	6663.4	4(2)	$(19/2^+) \rightarrow (17/2^+)$	
1402.4(9)	3580.1	7(3)	$(13/2^+) \rightarrow 9/2^+$	
1479.3(3)	3742.0	271(6)	$19/2^- \rightarrow 15/2^-$	1.12(6)
1511.9(6)	1602.7	51(12)	$7/2^+ \rightarrow 5/2^-$	
1524.4(6)	8365.7	15(2)	$(25/2^+) \rightarrow 25/2^-$	1.33(40)
1586.4(6)	2741.2	10(2)	$11/2^+ \rightarrow 9/2^-$	
1602.8(8)	1602.7	27(5)	$7/2^+ \rightarrow 7/2^-$	
1655.1(9)	9240.0	7(2)	$(27/2^+) \rightarrow (23/2^+)$	
1695.9(9)	5275.8	5(2)	$(17/2^+) \rightarrow (13/2^+)$	
1705.0(3)	2726.9	53(3)	$15/2^- \rightarrow 11/2^-$	1.32(24)
1705.3(6)	2859.9	6(2)	$13/2^- \rightarrow 9/2^-$	
1718.5(8)	7585.1	15(3)	$(23/2^+) \rightarrow (19/2^+)$	
1719.4(6)	2741.2	3(1)	$11/2^+ \rightarrow 11/2^-$	

TABLE I. (*Continued.*)

E_γ (keV)	E_i (keV)	I_γ^a	$I_i^\pi \rightarrow I_f^\pi$	R_{DCO}^b
1728.0(8)	8568.5	6(2)	$25/2^- \rightarrow 25/2^-$	
1730 ^c (1)	8568.5	16(2)	$25/2^- \rightarrow$	
1784.5(6)	5866.5	67(14)	$(19/2^+) \rightarrow (15/2^+)$	
1789.1(4)	5531.3	23(4)	$21/2^- \rightarrow 19/2^-$	0.51(14)
1834(1)	9419	4(2)	$(25/2^+) \rightarrow (23/2^+)$	
1837(1)	2859.9	3(1)	$13/2^- \rightarrow 11/2^-$	
1875.3(8)	7731.5	12(2)	$(23/2^+) \rightarrow 21/2^-$	
1916(1)	11155.5	25(4)	$(29/2^+) \rightarrow (27/2^+)$	
1946.1(3)	5688.1	480(11)	$23/2^- \rightarrow 19/2^-$	1.19(6)
1959.6(7)	10528.0	44(4)	$27/2^- \rightarrow 25/2^-$	0.57(25)
2043.9(7)	7731.5	9(2)	$(23/2^+) \rightarrow 23/2^-$	
2067.2(6)	6465.4	14(2)	$23/2^- \rightarrow 19/2^-$	
2114.0(5)	5856.1	88(3)	$21/2^- \rightarrow 19/2^-$	0.61(6)
2125(1)	5866.5	12(3)	$(19/2^+) \rightarrow 19/2^-$	
2178.6(8)	2178.0	12(4)	$9/2^+ \rightarrow 7/2^-$	
2200.2(6)	7731.5	17(2)	$(23/2^+) \rightarrow 21/2^-$	0.80(12)
2210(1)	10006	≈ 1	$(29/2^-) \rightarrow 27/2^-$	
2265.5(9)	6663.4	6(2)	$(19/2^+) \rightarrow 19/2^-$	
2416.7(8)	11656.8	24(3)	$(31/2^+) \rightarrow (27/2^+)$	
2558.3(8)	3580.1	4(2)	$(13/2^+) \rightarrow 11/2^-$	
2594(1)	13122	18(2)	$\rightarrow 27/2^-$	
2632(1)	7029.8	17(2)	$(21/2^+) \rightarrow 19/2^-$	0.76(10)
2723.1(7)	6465.4	13(2)	$23/2^- \rightarrow 19/2^-$	
2731(1)	10528.0	2(1)	$27/2^- \rightarrow 27/2^-$	
2880.3(7)	8568.5	29(2)	$25/2^- \rightarrow 23/2^-$	0.62(23)
2921(1)	6663.4	2(1)	$(19/2^+) \rightarrow 19/2^-$	
3096 ^c (1)	6838	16(2)	$\rightarrow 19/2^-$	
3165(1)	10006	4(2)	$(29/2^-) \rightarrow 25/2^-$	
3287(1)	7029.8	8(2)	$(21/2^+) \rightarrow 19/2^-$	0.47(4)
3687(1)	10528.0	2(1)	$27/2^- \rightarrow 25/2^-$	
4812(2)	12609	4(2)	$\rightarrow 27/2^-$	

^a γ -ray intensities have been obtained from spectra gated on the 90.6 and 1021.6 keV transitions and from branching ratios. The intensity of the 1021.6 keV line has been obtained from the γ - γ matrix projection.

^bDirectional correlation ratio determined from coincidence spectra, setting gates on stretched $E2$ transitions on both axes of the DCO matrix.

^cThe placement of the transition in the level scheme is not unambiguously fixed (see text).

has been reported populating a 3743 keV state [13]. The spin assignments for the yrast states at 6841.0 and 7796.5 keV are fixed at $25/2^-$ and $27/2^-$ at variance with Ref. [13], where they were assigned as $23/2^-$ and $25/2^-$, respectively. The transition feeding the state at 7801 keV reported in Ref. [13] has not been observed. Instead, the 7796.5 keV state is fed by the 4812 keV transition—the most energetic γ ray observed in the present work—, consistent with the assignment of the 7796.5 keV state as the band-terminating state.

III. DISCUSSION

The structure of ^{49}V has been interpreted in the framework of the shell model, which has shown to describe very accurately the nuclei in the $f_{7/2}$ shell [9,18]. Large scale calculations

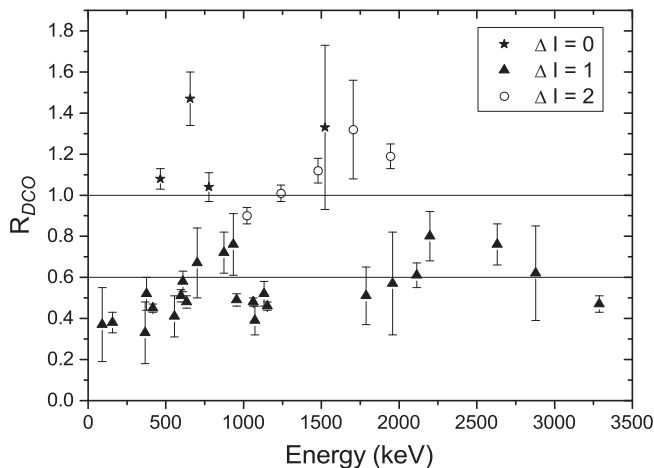


FIG. 3. Experimental DCO ratios. Horizontal lines correspond to theoretical values in the EUROBALL geometry for stretched quadrupole or $\Delta I = 0$ pure dipole transitions ($R_{DCO} \approx 1$) and $\Delta I = 1$ pure dipole transitions ($R_{DCO} \approx 0.6$).

were performed using the ANTOINE shell model code [19]. The natural parity levels have been obtained in the full fp shell using the effective interaction GXPF1A [20]. The results predict with very good accuracy the experimental data, as

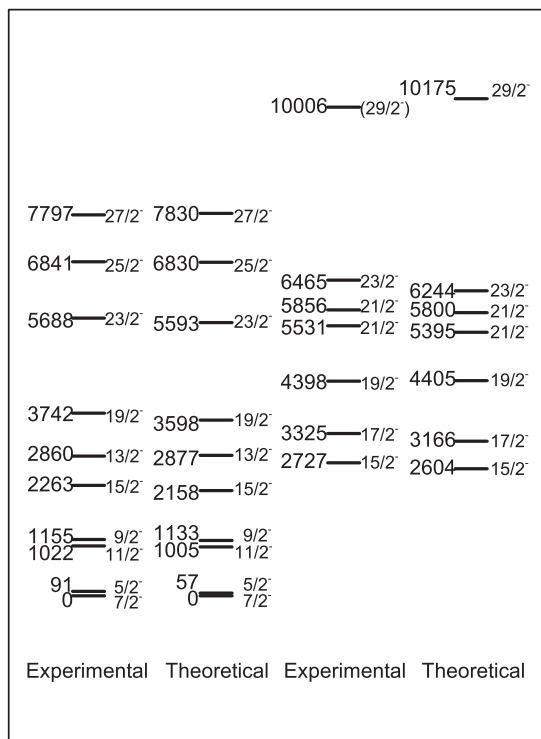


FIG. 5. Comparison between experimental negative-parity states and shell model predictions.

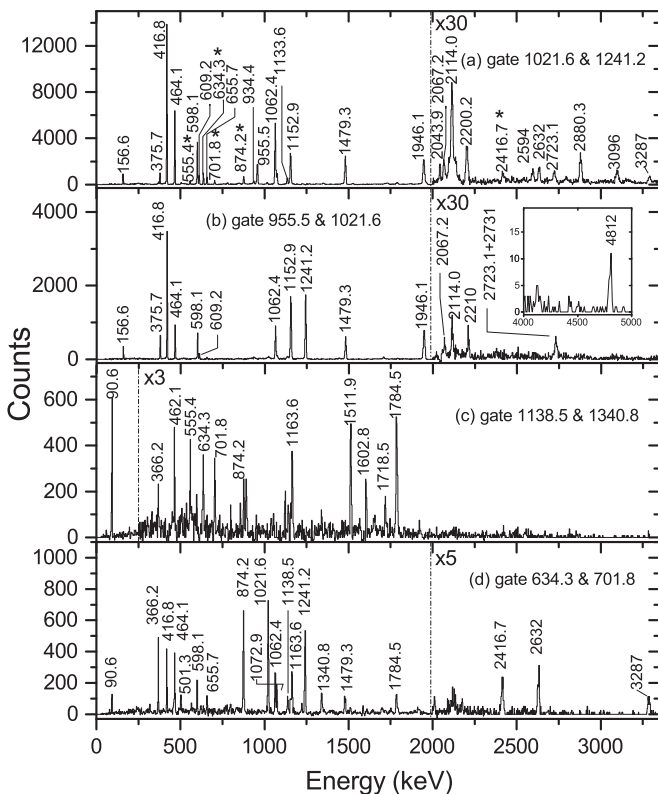


FIG. 4. Coincidence spectra gated on selected transitions which are indicated in each plot. In the upper panel, transitions marked with * correspond to the strongest transitions in the high spin structure on the upper right part of the level scheme. The inset in panel (b) corresponds to a compression of the spectrum by a factor of 4.

shown in Fig. 5. With the GXPF1A interaction, the states at high spin are better reproduced than using the same basis and code but with the effective interaction KB3G [21] according to the calculations performed in Ref. [18]. The $7/2^-$ ground state is very close to the $5/2^-$ state. This has been interpreted in Ref. [18] in terms of the Nilsson model as a fingerprint of a discrete deformation of ^{49}V at low spin. This is supported by the relatively high reduced electric quadrupole transition probabilities calculated for these states. In the same work, the authors suggest that the signature effects observed in the ground state band could be related to triaxiality.

A side band starts at the $15/2^-$ state at 2726.9 keV, which can be interpreted as a three quasiparticle structure [18]. This band mixes strongly with the ground state band which explains the observed depopulation of the 3742.0 keV state. In order to understand this behavior in the framework of the shell model, we have calculated the theoretical branching ratios for several yrast states and compared them with the experimental ones (see Table II). As can be seen, the depopulation pattern of states at 3742.0, 5688.1, 7796.5, and 10006 keV is predicted in agreement with the experimental results. In particular, for the 3742.0 keV state, the 416.8 keV transition is preferred instead of the 1479.3 keV one by a factor 1.6, in agreement with the factor 2 observed. On the other hand, we can use the information of Table II to explain why we do not observe a transition of 465 keV between the $17/2^-$ and $13/2^-$ states, present in the level scheme proposed by Cameron *et al.* [13]. The intensity expected for this transition is far below the detection limit of our experiment. The lower limits for the experimental branching ratios were calculated taking into

TABLE II. Experimental and theoretical branching ratios of several yrast states.

E_i (keV)	I_i^π	I_f^π	E_γ (keV)	$I_\gamma(I_i \rightarrow I_i-1)/I_\gamma(I_i \rightarrow I_i-2)$	
				Experimental	Theoretical
3325.2	$17/2^-$	$15/2^-_1$	1062.4	$> 4 \times 10^2$	5.4×10^5
		$15/2^-_2$	598.1	$> 2 \times 10^2$	1.5×10^5
		$13/2^-$	465 ^a		
3742.0	$19/2^-$	$17/2^-$	416.8	2	1.6
		$15/2^-$	1479.3		
5688.1	$23/2^-$	$21/2^-$	156.6	11×10^{-2}	2.7×10^{-2}
		$19/2^-$	1946.1		
		$23/2^-$	1331 ^a		
7796.5	$27/2^-$	$25/2^-$	955.5	$> 2 \times 10^2$	1.3×10^2
		$23/2^-$	1331 ^a		
10006	$29/2^-$	$27/2^-$	2210	0.25	0.13
		$25/2^-$	3165		

^aEnergy difference between states; transition not observed experimentally.

account the lowest intensity measured in this work (≈ 1 for the 2210 keV transition). Moreover, Fig. 6 shows the calculated DCO ratio as a function of the mixing parameter δ [16] and the experimental DCO ratio for the 416.8 keV transition, gating on the 1241.2 keV $15/2^- \rightarrow 11/2^-$ transition. The deduced value is $\delta^{\text{exp}} = -0.04(2)$. This agrees well with the theoretical value $|\delta^{\text{theor}}| = 0.03$ obtained from the γ -ray transition probabilities using the ANTOINE code.

The $I^\pi = 27/2^-$ state at 7797 keV excitation energy is identified as the terminating state of the ground-state band. This is the maximum spin that can be reached by aligning the valence particles in the $f_{7/2}$ shell to the maximum spin. Indeed, the calculated wave function has a dominant configuration with all the nine particles in the $f_{7/2}$ shell of about 90%.

We were unable to determine the DCO ratios of the weak 2210 and 3165 keV transitions depopulating the 10006 keV state. The assignment of $I^\pi = 29/2^-$ to this state is based on

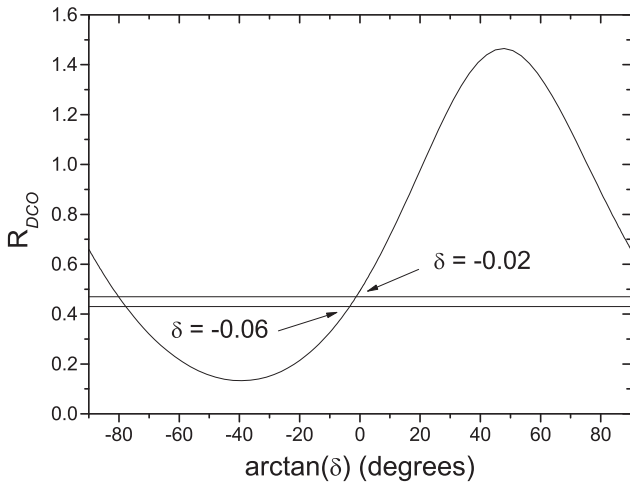


FIG. 6. Theoretical DCO ratio as a function of the mixing ratio for the 416.8 keV $19/2^- \rightarrow 17/2^-$ transition, gating on the 1241.2 keV $15/2^- \rightarrow 11/2^-$ transition. Horizontal lines correspond to the experimental DCO ratio limits.

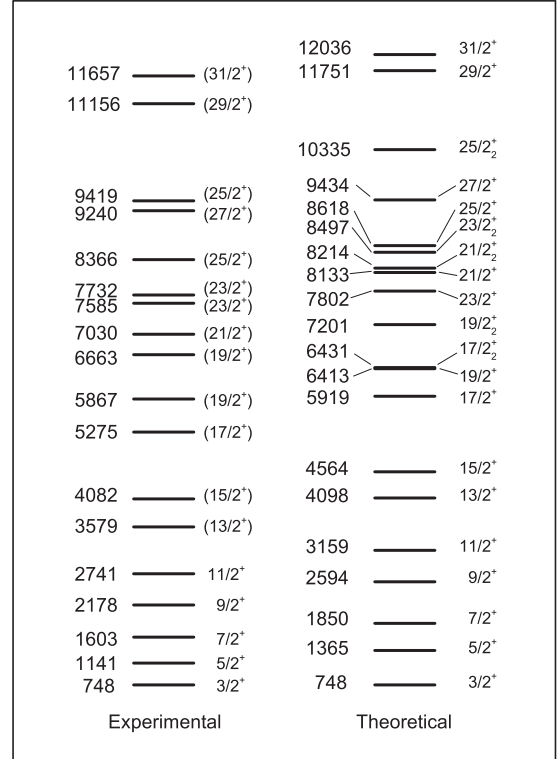


FIG. 7. Comparison between experimental positive-parity states and shell model predictions.

the fact that the theoretical value is predicted just 175 keV above and compatible with the decay pattern. In fact, the calculations predict that the probability to decay to the $25/2^-$ state is about 8 times larger than that to the $27/2^-$ state.

Calculations for the positive parity levels have been performed including the sd shell using the SDPF interaction [21], allowing the excitation of one nucleon from the $d_{3/2}$ orbit to the f p shell. Figure 7 compares the experimental and theoretical positive-parity states. The theoretical states are predicted to be slightly higher than the experimental ones, i.e., the calculated structure looks less collective than the experimental structure. All the observed positive-parity yrast states up to the first $I^\pi = 19/2^+$ are characterized by a main configuration with a particle-hole excitation of a proton from the $d_{3/2}$ orbital. In the second $I^\pi = 19/2^+$, a neutron excitation from the $d_{3/2}$ orbital to the $f_{7/2}$ one is more probable than a proton excitation. The $I^\pi = 21/2^+$ above this state has a mixed configuration and it is predicted to decay preferentially to the $I^\pi = 19/2^+$, in agreement with the experiment. The calculations agree with the observed decay pattern at higher spins in this structure with states connected with strong $M1$ transitions. The band terminates at the $I^\pi = 31/2^+$ state at 11657 keV with 75% of the wave function with ten particles in the $f_{7/2}$ shell and one proton $d_{3/2}$ hole, giving rise to the maximum aligned angular momentum.

IV. CONCLUSIONS

High spin states in ^{49}V have been populated via the $^{28}\text{Si}(^{28}\text{Si}, \alpha 3p)$ fusion evaporation reaction. A total of 87 γ -ray

transitions have been observed by using the EUROBALL IV γ -ray detector array and the Recoil Filter Detector, which allowed us to achieve a very high resolution due to the measurement of the direction of the recoils and their velocity. The proposed level scheme includes 21 states and 51 transitions observed for the first time in this work. Spin and parity of the states have been assigned on the basis of DCO ratios, decay patterns, and theoretical arguments. The high statistics and the quality of the data allowed us to significantly improve the previously known level scheme and to extend it to very high spin, above the band-termination

state. Theoretical calculations were performed with the shell model, which turned out to be very accurate for the description of both positive- and negative-parity structures up to the band-terminating states.

ACKNOWLEDGMENTS

This work has been partially supported by the European Union under contract ERBFMBICT-983127 and by the Polish National Science Centre (NCN) grants 2011/03/B/ST2/01894 and 2013/08/M/ST2/00591

-
- [1] S. M. Lenzi, D. R. Napoli, A. Gadea, M. A. Cardona, D. Hojman, M. A. Nagarajan, C. R. Alvarez, N. H. Medina, G. de Angelis, D. Bazzacco, M. E. Debray, M. de Poli, S. Lunardi, and D. de Acuña, High spin states in ^{48}Cr , *Z. Phys. A* **354**, 117 (1996).
- [2] S. M. Lenzi, C. A. Ur, D. R. Napoli, M. A. Nagarajan, D. Bazzacco, D. M. Brink, M. A. Cardona, G. de Angelis, M. De Poli, A. Gadea, D. Hojman, S. Lunardi, N. H. Medina, and C. Rossi Alvarez, Band termination and second backbending in ^{50}Cr , *Phys. Rev. C* **56**, 1313 (1997).
- [3] S. M. Lenzi, C. A. Ur, D. R. Napoli, D. Bazzacco, F. Brandolini, J. A. Cameron, G. de Angelis, M. De Poli, E. Farnea, A. Gadea, S. Lunardi, G. Martínez-Pinedo, A. Poves, C. Rossi Alvarez, H. Somacal, and C. E. Svensson, Structure of $N = Z$ nuclei in the $1f_{7/2}$ shell, *Nuovo Cimento A* **111**, 739 (1998).
- [4] J. A. Cameron, J. Jonkman, C. E. Svensson, M. Gupta, G. Hackman, D. Hyde, S. M. Mullins, J. L. Rodriguez, J. C. Waddington, A. Galindo-Uribarri, H. R. Andrews, G. C. Ball, V. P. Janzen, D. C. Radford, D. Ward, T. E. Drake, M. Cromaz, J. DeGraaf, and G. Zwartz, Collective properties of ^{48}Cr at high spin, *Phys. Lett. B* **387**, 266 (1996).
- [5] S. M. Lenzi, D. R. Napoli, C. A. Ur, D. Bazzacco, F. Brandolini, J. A. Cameron, E. Caurier, G. de Angelis, M. De Poli, E. Farnea, A. Gadea, S. Hankonen, S. Lunardi, G. Martínez-Pinedo, Z. Podolyak, A. Poves, C. Rossi Alvarez, J. Sánchez-Solano, and H. Somacal, Band termination in the $N = Z$ odd-odd nucleus ^{46}V , *Phys. Rev. C* **60**, 021303 (1999).
- [6] E. Caurier, J. L. Egido, G. Martínez-Pinedo, A. Poves, J. Retamosa, L. M. Robledo, and A. P. Zuker, Intrinsic vs Laboratory Frame Description of the Deformed Nucleus ^{48}Cr , *Phys. Rev. Lett.* **75**, 2466 (1995).
- [7] F. Brandolini, S. M. Lenzi, D. R. Napoli, R. V. Ribas, H. Somacal, C. A. Ur, D. Bazzacco, J. A. Cameron, G. de Angelis, M. De Poli, C. Fahlander, A. Gadea, S. Lunardi, G. Martínez-Pinedo, N. H. Medina, C. Rossi Alvarez, J. Sánchez-Solano, and C. E. Svensson, Precise DSAM lifetime measurements in ^{48}Cr and ^{50}Cr as a test of large scale shell model calculations, *Nucl. Phys. A* **642**, 387 (1998).
- [8] E. Caurier, A. P. Zuker, A. Poves, and G. Martínez-Pinedo, Full pf shell model study of $A = 48$ nuclei, *Phys. Rev. C* **50**, 225 (1994).
- [9] G. Martínez-Pinedo, A. P. Zuker, A. Poves, and E. Caurier, Full pf shell study of $A = 47$ and $A = 49$ nuclei, *Phys. Rev. C* **55**, 187 (1997).
- [10] I. Ragnarsson, V. P. Janzen, D. B. Fossan, N. C. Schmeing, and R. Wadsworth, Smooth Termination of Collective Rotational Bands, *Phys. Rev. Lett.* **74**, 3935 (1995).
- [11] S. Frauendorf, J. A. Sheikh, and N. Rowley, Consequences of neutron-proton interactions on backbending, *Phys. Rev. C* **50**, 196 (1994).
- [12] S. M. Lenzi, Nuclear properties and underlying symmetries in deformed $f_{7/2}$ -shell nuclei, *Nucl. Phys. A* **704**, 124 (2002).
- [13] J. A. Cameron, M. A. Bentley, A. M. Bruce, R. A. Cunningham, W. Gellately, H. G. Price, J. Simpson, D. D. Warner, and A. N. James, High-spin gamma spectroscopy of recoil-separated ^{49}Cr , ^{49}V , and ^{46}Ti , *Phys. Rev. C* **44**, 1882 (1991).
- [14] C. Rossi Alvarez, The EUROBALL array, *Nuovo Cimento A Ser.* **111**, 601 (1998).
- [15] W. Męczyński, P. Bednarczyk, J. Grębosz, J. Heese, M. Janicki, K. Maier, J. Merdinger, K. Spohr, M. Ziębliński, and J. Styczeń, A detector for filtering x-ray spectra from weak fusion-evaporation reactions out of strong background and for doppler correction: The recoil filter detector RFD, *Nucl. Instrum. Methods Phys. Res., Sect. A* **580**, 1310 (2007).
- [16] K. S. Krane, R. M. Steffen, and R. M. Wheeler, Directional correlations of gamma radiations emitted from nuclear states oriented by nuclear reactions or cryogenic methods, *Nucl. Data Tables* **11**, 351 (1973).
- [17] T. Burrows, Nuclear data sheets for $a = 49$, *Nucl. Data Sheets* **109**, 1879 (2008).
- [18] F. Brandolini and C. A. Ur, Shell-model description of $n \simeq z1.f_{7/2}$ nuclei, *Phys. Rev. C* **71**, 054316 (2005).
- [19] E. Caurier and F. Nowacki, Present status of shell model techniques, *Acta Phys. Pol. B* **30**, 705 (1999).
- [20] M. Honma, T. Otsuka, B. A. Brown, and T. Mizusaki, Shell-model description of neutron-rich pf-shell nuclei with a new effective interaction GXPF 1, *Eur. Phys. J. A* **25**, 499 (2005).
- [21] A. Poves and J. S. Solano, Positive-parity rotational bands in odd- A pf-shell nuclei: A shell model description, *Phys. Rev. C* **58**, 179 (1998).